

An angle-resolved soft x-ray spectroscopy study of the electronic states of single crystal MgB₂

G. P. Zhang,^{1,2,*} G. S. Chang,¹ T. A. Callcott¹

¹*Department of Physics and Astronomy, The University of Tennessee at Knoxville, TN 37996*

²*Department of Physics, Indiana State University, Terre Haute, IN 47809**

D. L. Ederer

Physics Department, Tulane University, New Orleans, LA 70118

W. N. Kang, Eun-Mi Choi, Hyeong-Jin Kim, Sung-Ik Lee

National Creative Research Initiative Center for Superconductivity and Department of Physics, Pohang University of Science and Technology, Pohang 790-784, Korea

(June 24, 2018)

Angle-resolved soft x-ray measurements made at the boron K-edge in single crystal MgB₂ provide new insights into the B-2p local partial density of both unoccupied and occupied band states. The strong variation of absorption with incident angle of exciting x-rays permits the clear separation of contributions from σ states in the boron plane and π states normal to the plane. A careful comparison with theory accurately determines the energy of selected critical k points in the conduction band. Resonant inelastic x-ray emission at an incident angle of 15° shows a large enhancement of the emission spectra within about 0.5 eV of the Fermi level that is absent at 45° and is much reduced at 60°. We conclude that momentum transferred from the resonant inelastic x-ray scattering (RIXS) process couples empty and filled states across the Fermi level.

74.25.Jb, 71.20.-b, 78.70.Dm, 78.70.En

I. INTRODUCTION

The discovery of superconductivity in MgB₂ came as a surprise.¹ Its unusually high transition-temperature immediately motivated intensive investigations. Although the conventional BCS mechanism most likely underlies this peculiar superconductivity, the precise mechanisms are less clear. Different sample qualities and different experimental techniques show inconsistent gap values ranging from 2 meV to 7 meV.² However, in a single crystal sample, results are less ambiguous. A recent angle-resolved photoemission (PE) study on a small MgB₂ single crystal showed detailed dispersion of the occupied band along the $\Gamma - K$ and $\Gamma - M$ directions.³ However, due to the large background and low intensity for normal emission, the dispersion along the k_z -direction was not resolved.

Soft x-ray absorption (SXA) spectroscopy⁴ complements PE by providing an element and angular momentum selected local, partial density of states (LPDOS) of the unoccupied bands. Similarly, soft x-ray fluorescence (SXF) spectra provide a measure of the LPDOS for the occupied valence bands. Although these spectroscopies are not generally selective for momentum, they can often provide an accurate measure of density of states features associated with critical points of the band structure and thus provide a detailed check on theoretical band calculations. These features of x-ray spectroscopies are clearly illustrated in a recent paper (the first paper of Ref. [5]) on MgB₂,⁵ which used SXF and SXA studies to map the

boron p-LPDOS for a polycrystalline sample.

We have recently shown that in an anisotropic material such as NaV₂O₅,⁶ additional selectivity can be obtained by varying the incident angle of the exciting x-rays.⁷ By varying the incident angle of exciting x-rays so that the polarization vector is varied with respect to a bond direction, it is possible to selectively excite electrons to electronic orbitals having particular spatial orientation. In this paper, we report angle resolved soft x-ray absorption and emission measurements at the boron K -edge of a single crystal film of MgB₂. The soft x-ray absorption spectra provide a measure of the B-2p LPDOS for unoccupied states above the Fermi level. The angular resolved spectra allow us to separate excitation to band states derived from B σ states directed within the boron plane and π states directed perpendicular to the plane. The results enable us to identify critical points of unoccupied band states along several crystal-momentum directions, which can be directly compared to our theoretical calculations.

For excitation near a band edge, the excitation and emission processes may be coupled so that the emission spectra must be interpreted in terms of a resonant inelastic x-ray scattering (RIXS) process. In the RIXS process incident x-rays excite electronic excitations and are scattered with reduced energy. Previous RIXS experiments in graphite,⁸ diamond, silicon, cBN⁹ and hBN¹⁰ show that in well screened and delocalized electronic systems the momentum conservation inherent in the RIXS process can provide direct information about band dispersion. These analyses generally assume that the momen-

tum transferred in the RIXS process is small on the scale of the Brillouin zone so that the electronic excitations induced by RIXS are nearly vertical in the reduced zone. In MgB_2 , however, we observe a strong enhancement of a narrow band of states near the top of the occupied band that requires an electronic excitation across the Fermi level and thus a transfer of momentum. The variation of this enhancement with incident angle demonstrates that the enhancement is a result of momentum transfer from the RIXS process, and not primarily associated with other processes such as phonon-assisted transitions that might allow momentum to be conserved.

The paper is arranged as follows. In Section II, we present the angular-resolved absorption spectra. The angular-resolved RIXS spectra are presented in Section III.

II. ANGULAR RESOLVED X-RAY ABSORPTION SPECTRA

A single crystal of MgB_2 was grown as a thin film of 400 nm thickness on the R -plane (1 $\bar{1}$ 02) of an Al_2O_3 substrate.¹¹ An amorphous B thin film was deposited by pulsed laser deposition and a high-quality and single crystal MgB_2 film was obtained by sintering the thin film at 900°C for 20 minutes in Mg vapor. The crystal quality and orientation was confirmed by x-ray diffraction. The process is described in detail elsewhere.¹¹ The dc magnetization measured with a superconducting quantum interference device (SQUID) magnetometer showed that the superconducting transition temperature (T_c) is 39 K, and the 10-90% transition width is 0.7 K. Our soft x-ray measurements were made at room temperature at Beamline 8.0 of the Advanced Light Source at Lawrence Berkeley National Laboratory. The slits of the beamline monochromator were set to provide a resolution of about 0.1 eV for the absorption spectra, while the resolution of the emission spectrometer is about 0.2 eV at the 190 eV energy of the Boron K spectra.

The experimental geometry is indicated in Fig. 1. MgB_2 is a layered compound with alternating layers of boron and Mg stacked along the c axis. Graphite-like hexagonal layers of boron lie in the $a-b$ plane. Linearly polarized x-ray light from an undulator and monochromator was incident on the sample. By rotating the sample holder, we can scan the polarization vector from the $a-b$ plane toward the c axis with θ changed from 15° to 45°. θ measures the angle between the incident x-ray beam and the sample normal as well as the angle between the polarization vector of incident photons and the $a-b$ plane.

Figure 2(a) shows the dramatic change of the absorption spectra measured in total fluorescent yield mode with θ . The spectra shown are taken at 7.5° intervals from 15° to 45° with angles measured from the $a-b$ plane. The experimental spectra of Fig. 2(a) are normalized with respect to the total areas from 183.55 to

208.55 eV (boron K -edge). Experimental and theoretical spectra are aligned with peak labeled a . The Fermi level is set to zero (long dashed line). The zero energy corresponds to an energy of 187.28 eV with uncertainty of about 1 eV in the absolute energy, consistent with our previous measurement.⁵ The relative energies of emission and absorption spectra are calibrated to be accurate to about 0.1 eV. Figure 2 shows that the Fermi level cuts through the pre-edge of peak a , a result which agrees with the photoemission data³ and shows normal metallic behavior. We identify six spectral features labeled from a to f . At $\theta = 15^\circ$, only two peaks a and f are observable leaving a 4 eV-wide valley from 1 eV to 5 eV. As the polarization rotates from the $a-b$ plane toward the c axis, peak a grows slightly while peak f drops. The most remarkable change is in the valley where the whole valley is gradually filled. We will concentrate on the two broad peaks at 2.2 and 2.8 eV above the Fermi level, which increase in amplitude to a point comparable to peak a . We note here that in a polycrystalline or powder sample these angular dependent changes in the absorption spectra are not observed because they are intrinsically angle averaged.¹²

Our calculated *ab initio* results are shown in Fig. 2(b), where we also present two additional spectra at $\theta = 0^\circ$ and 90° . For an easy comparison, we plot spectra calculated for the exact same experimental conditions. The angular variation results from explicit calculation of the dipole matrix elements taking into account the projection of the polarization vector on the orbital amplitude in real space. The theoretical calculations have been described in greater detail in a recent paper on NaV_2O_5 .⁷ In brief, we calculate the eigenvalues and wavefunctions by solving the Kohn-Sham equation,

$$\hat{H}\Psi_{n\mathbf{k}}(\mathbf{r}) = \left\{-\frac{\hbar^2}{2m}\nabla^2 + \hat{V}_{\text{eff}}\right\}\Psi_{n\mathbf{k}}(\mathbf{r}) = E_{n\mathbf{k}}\Psi_{n\mathbf{k}}(\mathbf{r}). \quad (1)$$

Then, we compute transition matrix elements between the core level and unoccupied bands. It is quite impressive that the theoretical spectra reproduce the experimental ones very accurately. Both the overall shape and peaks and valleys are consistent with the experimental counterparts. A quantitative comparison is given in Table I. One notices that except for peak f , theoretical results for peaks and valleys from b to e are about 0.2 eV larger than the experimental ones, which may suggest band narrowing possibly due to correlation effects. This band narrowing, if real, is much smaller than the simple metals such as Na, Li and Mg,¹³ especially considering the experimental uncertainty of about 0.2 eV. In any case, the effect is small.

A. Incident at $\theta = 15^\circ$

The good agreement between theory and experiment paves the way for a detailed investigation of the origin of

the peaks. To help our analysis, we draw several vertical short-dashed lines across both the absorption spectra [Figs. 2(a) and 2(b)] and the band structure [Fig. 2(c)] to highlight important connections. We label those crossing points of peaks a , c , d and f by a_1 , a_2 , etc. With an incident angle of 15° , the polarization vector is 15° from the $a - b$ plane, so that we mostly probe the σ -orbitals directed between B atoms lying in the a - b plane. For excitation to states within 0.5 eV of the absorption edge, we see from the spectra that only peak a is excited. Now comparing with the band structure, we can see six different points from a_1 to a_6 which potentially contribute to this peak and distribute almost evenly along all momentum directions. For instance, points a_1 and a_4 in Fig. 2(c) fall near the Γ point along the $\Gamma - M$ and $\Gamma - K$ lines respectively, while a_2 is close to the M_1 point. a_3 is almost in the middle of the $\Gamma - K$ line, and a_5 , representing two nearby points along the $A - L$ line, is close to the A point, whereas a_6 along the $A - L$ line is close to the L point.

If we solely depended on the energy position, we would not be able to resolve these different band contributions to the a peak, a common complication in soft x-ray spectroscopy. Fortunately, MgB_2 is highly anisotropic so that there are strong variations in the angular dependent transition matrix elements that allow us to resolve the contributions from different bands. We can use the transition matrix elements $\langle \psi_{nk}(r) | \vec{E} \cdot \vec{r} | \psi_{B1s}(r) \rangle$ to resolve these features, where $|\psi_{nk}(r)\rangle$ is the band state and $|\psi_{B1s}(r)\rangle$ is the boron 1s core level. Transition matrix elements contain both the direct space and reciprocal space information, which helps us to probe the spatial orientation of orbitals and reveal the dispersive band in momentum space.

In Fig. 3, in the upper part, we show the BZ in the three dimension, while in the lower part, we plot the calculated transition matrix elements at various positions in the BZ and for different angles of the incident light. The four columns represent the transition matrix elements for four peaks from a to f in the momentum space. Rows 1 and 2 refer to $k_z = 0$ plane at the bottom of the BZ which contains the Γ point while 3 and 4 refer to $k_z = 2\pi/c$ plane at the top of the BZ which contains the A point (see the top graph in Fig. 3). The first and third rows refer to the results at $\theta = 15^\circ$, while the second and fourth ones the results at $\theta = 45^\circ$. The high symmetry k points are also indicated in Figs. 3(a) and 3(c) for the top and bottom planes. Numbers near the contours in Fig. 3 indicate the magnitude of transition matrix elements (in arbitrary units). First focus on Figs. 3(a) and 3(c), which show the matrix elements contribution to peak a for $\theta = 15^\circ$. From those two figures, one can see clearly that the largest transition matrix elements are well localized at the Γ point and in the vicinity of the A point while contributions from other directions are very small. In three dimensions, it is found that the matrix elements remain equally strong for the region surrounding the $\Gamma - A$ line that lies within the tubular Fermi

surface¹⁴ that surrounds this line (see the top graph of Fig. 3). Returning to Fig. 2(c), now we can identify that band states at $a_1(a_4)$ and a_5 contribute most strongly to peak a . Therefore, the position of peak a can be used to measure the position for Γ_1 , which is 0.27 eV above the Fermi surface. Our assignment is also consistent with the nature of the σ band along the $\Gamma_1 - A_1$ line. It is well known that this famous σ band is derived from electronic orbitals in the $a - b$ plane. Since our present electric field polarization is nearly in the $a - b$ plane, this band is strongly excited.

If we increase the incoming photon energy to 0.69 eV (with respect to the Fermi level), the spectra start to fall sharply since there is no density of states above A_1 and bands along $M - K - \Gamma$ can not be effectively excited (see below). When we increase the photon energy further up to the Γ_2 point, we begin to access a new band (c_4 and c_5 , or d_4 and d_5), thus we would expect a strong increase of the spectral weight. Surprisingly, we see a 4 eV-wide valley instead. The valley also appears in the theoretical spectra (see Fig. 2(b)). The transition-matrix element contours in Figs. 3(e) and 3(g) are for peak c , and in Figs. 3(i) and 3(k) for peak d , but the matrix elements are small.

In order to obtain a qualitative understanding of these variations in the matrix elements, we calculated the spatial charge density distribution. For the bands at point c_6 (similarly d_6 , c_2 and c_3), we find that they are derived from π -orbitals and are highly oriented along the c axis (see Fig. 4(a)), which explains why they can not be effectively excited. However, this does not explain bands at points c_4 , c_5 , d_4 and d_5 since they do lie in the $a - b$ plane (see Fig. 4(b)). A very careful investigation reveals the secret: those orbitals in Fig. 4(b) are strongly localized around Mg sites, not B sites. Since our measurement is element-specific and is done at the boron K edge, we are not sensitive to orbitals around the Mg sites, which explains the appearance of the 4-eV wide valley at $\theta = 15^\circ$.

Above the valley labeled e at 3.66 eV, the spectra increase in intensity. Further increasing the photon energy to 6.0 eV above the Fermi level, we pick up high-lying σ bands along the $\Gamma_3 - A_2$ direction and the $\Gamma - K$ (A - L) line. This can be seen directly from the transition-matrix contour plot in Figs. 3(m) and 3(o). Therefore, the energy position of peak f is a good measure of the position of the Γ_3 and A_2 points. Our experiment gives the value of 6.65 eV, which can be compared with the theoretical value of 6.55 eV.

B. Incident at $\theta = 45^\circ$

When we rotate the polarization vector from the $a - b$ plane toward the c axis ($\theta = 45^\circ$), we begin to probe orbitals which are oriented along the c axis. We start from peak a . Comparing Figs. 3(a) with 3(b) (Figs. 3(c) with

3(d)), one notices that the spectral weight moves away from the Γ (A) point to the M-K (H-L) line. Qualitatively we can say that the contribution to this peak from the σ -bands is decreasing with angle while the contribution from the π -bands is strongly increasing. Clearly, these angular measurements give us the ability to cleanly separate the contribution of bands with different spatial orientation to the measured density of states.

As the angle is increased, two broad peaks c and d appear at 2.2 and 2.8 eV above the Fermi surface (see Figs. 2(a) and 2(b)), respectively. Although there are six crossing points contributing to peak c , we can safely exclude c_1 , c_4 and c_5 since they are from Mg sites. The transition matrix contour in Fig. 3(f) shows that states with large elements are near the K point, while at $k_z = 2\pi/c$, the matrix elements are only half that of the states at $k_z = 0$ (see Fig. 3(h)). Therefore, peak c predominantly comes from states at c_2 and c_3 and determines their energy positions. The momenta for these states are (0.38,0.25,0) and (0.3,0.3,0), respectively. They form a hot spot which leads to peak c . For peak d , the transition matrix contour plot (see Fig. 3(j)) shows that the dominant contribution comes from states along the $M - K$ and $\Gamma - K$ lines. States at d_4 and d_5 (see Fig. 2(c)) do not contribute because those states originate from Mg sites. The main contribution is from bands at d_2 and d_3 which are highly oriented along the c axis (see Fig. 4(a)). They form another hot spot which ultimately leads to peak d . By carefully analyzing the data, we find that point d_3 is at (0.28, 0.28, 0) in the reciprocal space while point d_2 is at (0.46, 0.09, 0), very close to the M point. The position of peak d of 2.8 eV is a good measure of the energy position for the M_2 point.

Summarizing all the data, we tabulate in the last column of Table I the measured values of unoccupied band states at selected points of both high and low symmetry in k-space. These measured values of particular points in k-space provide values that may be compared directly to calculated values.

III. ANGLE RESOLVED RESONANT INELASTIC SCATTERING

We now turn our attention to the soft x-ray (SX) emission spectra produced when electrons from occupied valence states refill the excited core state. Well above the excitation threshold, the excitation and emission processes are always decoupled so that the normal SX fluorescence (SXF) spectra represent the boron p-LPDOS of the filled valence band. Near threshold, however, the absorption and emission processes are often strongly coupled and must be described in terms of a resonant inelastic x-ray scattering (RIXS) process. An important defining feature of RIXS spectra is that the energy difference between incident and scattered electrons is equal to the energy of the electronic excitations so that RIXS

features move in energy with the excitation energy, while normal SXF features remain fixed in energy. For near threshold excitation, normal SXF and RIXS are often superimposed. In the present data, resonant features in the SXF spectra are observed near threshold for excitation to the σ states that contribute to peak a in Fig. 2. For energies more than 1 eV above the absorption threshold, the spectra do not change with further increases in energy and are representative of SXF spectra.

The emission spectra are presented in Fig. 5 for excitation energies within 1 eV of the boron K edge. Note that the Fermi level is at about 187.28 eV. Spectra are shown for incident angles of 15° and 60° . Figure 5(a) shows the results at 15° where we have seen that excitation is mainly into the σ states. When we excite at 187.25 eV, only an elastic peak A can be seen. Increasing the excitation energy to the threshold of 187.50 eV, a shoulder appears on the low energy edge of A and a broad peak B appears around 185.05 eV. Its energy position stays the same even with higher excitation energies of 188.00 and 188.25 eV, which identifies it as a normal fluorescence peak, where the excitation and de-excitation processes are decoupled.

From Fig. 5(a), we notice that at the excitation energy of 187.50 eV, the elastic peak A becomes asymmetric and broader. The shape of its left shoulder indicates a possible peak hidden there. This is indeed the case. When we further increase the excitation energy to 187.75 eV, peak C is revealed at 187.30 eV. Two significant features of this peak may be noted. The strong resonant enhancement of the peak remains visible so long as absorption is into the σ -band and ends when the excitation energy exceeds the A_1 point of this band (see Fig. 2). The resonance region extends only to about 1 eV below the Fermi edge and thus does not include the lower energy σ states. With excitation at an incident angle of 60° shown in Fig 5(b), the resonant enhancement is greatly reduced, but is still present. For excitation at 45° (not shown), no enhancement at all is observed in the SXF spectra. Comparing Figs. 5(a) with 5(b), we find that they are very similar, and within our experimental resolution of 0.2 eV the peak positions are identical (see Table II). The only significant difference is the reduction in the magnitude of the resonant enhancement near the Fermi level when the angle is increased from 15° to greater angles.

It is difficult to account for the resonant enhancement in terms of an ordinary RIXS process in a delocalized system, because k-conservation is expected for the two photon scattering process. K-conservation follows from the Kramers-Heisenberg formula that describes the RIXS process⁶

$$S(\omega, \omega') \propto \sum_f \left| \sum_m \frac{\langle f|p \cdot A|m\rangle \langle m|p \cdot A|gs\rangle}{\omega + E_{gs} - E_m - i\Gamma} \right|^2 \times \delta(E_{gs} + \omega - E_f - \omega'), \quad (2)$$

where $|gs\rangle$, $|m\rangle$, and $|f\rangle$ are initial, intermediate, and

final states, and E_{gs} , E_m , and E_f are their energies, respectively; ω and ω' are the incident and emitted photon energies; Γ is the spectral broadening due to the core lifetime in the intermediate state. $p \cdot A$ is the transition operator. If $|\psi_{nk_1}\rangle$ is the intermediate state $|m\rangle$ with momentum k_1 and $|\psi_{nk_2}\rangle$ is the final state $|f\rangle$ with momentum k_2 , besides the energy conservation, the total momentum should be conserved, i.e., $q + k_1 = q' + k_2$, where q and q' are momenta for the incoming and outgoing photons, respectively. If the photon momenta q and q' were negligible as is the case in visible spectroscopy, we would have $k_1 \approx k_2$ or zero momentum transfer.

Previous calculations¹⁴ show that the empty states from the σ band lie in a small tubular region in k-space surrounding the Γ -A axis,¹⁴ while the filled states from this band are located outside of this tube. This behavior can also be seen for the Γ -K, Γ -M and A-L axes in Fig. 2(c) and are similar for all other directions normal to the Γ -A axis. Thus the resonant enhancement requires a mechanism that provides momentum normal to this axis and couples the empty states inside the tube to the filled states outside the tube.

First, we will estimate the magnitude of the energy loss and momentum transfer for the enhanced emission. When excited at 187.75 eV, the resonant inelastic peak C in Fig. 5(a) has the energy loss that is centered at about 0.5 eV and covers a range of about 1 eV. To excite this range of energies requires a momentum transfer in the range of 0.1 on the scale of $2\pi/a$ which sets the scale of the BZ. All subsequent momentum values are quoted on this scale.

We have considered two possible processes that might provide the required momentum. They are phonon assisted transitions and momentum transfer from the RIXS scattering process.¹⁵ A previous calculation of the phonon spectrum¹⁶ shows that the in-plane phonon mode E_{2g} has a very strong electron-phonon coupling (EPC) along the Γ -A, Γ -M, and A-L directions. Such a strong but selective coupling might provide way to transfer momentum from the phonon subsystem to the electronic subsystem. Since there is no valence state available along the Γ -A direction, its strong coupling is irrelevant to the anomalous enhancement. The most important coupling is along the Γ -M and A-L directions. To be more specific, the in-plane E_{2g} phonon mode with the strongest EPC is the most important¹⁶. Along the Γ -M direction, phonon can transfer momentum \mathbf{q} to maximum values of (0.15,0,0), while along the A-L direction, transfers occur to maximum values of $\mathbf{q} = (0.2, 0, 0.5)$. These momentum transfers are of the correct order of magnitude to efficiently couple the excitation and de-excitation processes.

Since momentum is transferred in the SX scattering process, we also considered the possibility that this accounts for the observed enhancement. As indicated in Fig. 6(a), the scattering of X-ray photons through 90° requires a transfer of momentum in the interaction with the surface along a line 45° from the incident direction.

For 15° angle of incidence on the sample, the momentum transfer normal to the Γ -A line is calculated to be about $0.03 (2\pi/a)$, while for a 45° angle of incidence, there is no momentum transfer normal to this line. The mechanism is illustrated schematically in Fig. 6(b).

The variation of the magnitude of the resonant enhancement as the incident angle is varied allows us to choose between these two mechanisms. A phonon-assisted process should not depend on angle so that the enhancement in the spectra should only be reduced moderately by the change in the projection of the polarization on the σ orbitals in the $a - b$ plane. If the momentum is provided by the RIXS scattering process, the enhancement should be absent at 45° and greatly reduced at 60° . The measured enhancement is indeed found to be unobservable at 45° and greatly reduced at 60° . We conclude that the enhancement is enabled by the momentum provided by the RIXS process, allowing non-vertical transitions within the BZ.

We note finally that two separate angular dependent effects are present in the RIXS spectra. First the projection of the polarization vector of the incident x-rays on the orbitals determines the intensity of the absorption into the derived intermediate states. This factor falls off as a function of $\cos\theta$ with increasing incident angle. And second, the resonant enhancement near threshold depends on the momentum transfer perpendicular to the $\Gamma - A$ axis provided by the RIXS process, which varies as $\cos(\theta - 45^\circ)$ with a 90° scattering angle. A new experimental endstation will soon be available that will permit the scattering angle in RIXS measurements to be varied over a wide range, which will greatly facilitate the study of momentum transfer effects.

We acknowledge many helpful discussions with Eric L. Shirley. This research is supported by NSF Grant No. DMR-9801804. Measurements were carried out at the Advanced Light Source at LBNL supported by DOE contract DE-A003-76SF00098. This work is also supported in part by the Ministry of Science and Technology of Korea through the Creative Research Initiative Program.

*Mailing address.

-
- ¹ J. Nagamatsu, N. Nakagawa, T. Muranaka, Y. Zenitani, and J. Akimitsu, Nature (London) **63**, 410 (2001).
 - ² G. Karapetrov, M. Iavarone, W. K. Kwok, G. W. Crabtree, and D. G. Hinks, Phys. Rev. Lett. **86**, 4374 (2001); G. Rubio-Bollinger, H. Suderow, and S. Vieira, Phys. Rev. Lett. **86**, 5582 (2001).
 - ³ H. Uchiyama, K. M. Shen, S. Lee, A. Damascelli, D. H. Lu, D. L. Feng, Z.-X. Shen, and S. Tajima, Phys. Rev. Lett. **88**, 157002 (2002).
 - ⁴ T. A. Callcott, in Vacuum Ultraviolet Spectroscopy II, edited by J. A. Samson and D. L. Ederer, Experimental

Methods in the Physical Sciences, Vol. 32 (Academic Press, New York, 1998), pp. 279-300.

- ⁵ T. A. Callcott, L. Lin, G. T. Woods, G. P. Zhang, J. R. Thompson, M. Paranthaman, and D. L. Ederer, Phys. Rev. B **64**, 132504 (2001); E. Z. Kurmaev, I. I. Lyakhovskaya, J. Kortus, A. Moewes, N. Miyata, M. Demeter, M. Neumann, M. Yanagihara, M. Watanabe, T. Muranaka, and J. Akimitsu, Phys. Rev. B **65**, 134509 (2002).
- ⁶ G. P. Zhang, T. A. Callcott, G. T. Woods, L. Lin, Brian Sales, D. Mandrus and J. He, Phys. Rev. Lett. **88**, 077401 (2002); **88**, 189902 (2002, Erratum).
- ⁷ G. P. Zhang, G. T. Woods, Eric L. Shirley, T. A. Callcott, L. Lin, G. S. Chang, B. C. Sales, D. Mandrus, and J. He, Phys. Rev. B **65**, 165107 (2002); G. T. Woods, G. P. Zhang, T. A. Callcott, L. Lin, G. S. Chang, B. Sales, D. Mandrus, and J. He, Phys. Rev. B **65** 165108 (2002).
- ⁸ J. A. Carlisle, Eric L. Shirley, E. A. Hudson, L. J. Terminello, T. A. Callcott, J. J. Jia, D. L. Ederer, R. C. C. Perera, and F. J. Himpsel, Phys. Rev. Lett. **74**, 1234 (1995).
- ⁹ E. L. Shirley, J. A. Soininen, G. P. Zhang, J. A. Carlisle, T. A. Callcott, D. L. Ederer, L. J. Terminello and R. C. C. Perera, J. El. Spectr. & Rel. phenomena **114-116**, 939 (2001).
- ¹⁰ J. A. Carlisle, Eric L. Shirley, L. J. Terminello, J. J. Jia, T. A. Callcott, D. L. Ederer, R. C. C. Perera, and F. J. Himpsel, Phys. Rev. B **59**, 7433 (1999); J. Jia, T. A. Callcott, Eric L. Shirley, J. A. Carlisle, L. J. Terminello, A. Asfaw, D. L. Ederer, F. J. Himpsel, and R. C. C. Perera, Phys. Rev. Lett. **76**, 4054 (1996).
- ¹¹ W. N. Kang, Hyeong-Jin Kim, Eun-Mi Choi, C. U. Jung, and Sung-Ik Lee, Science **292**, 1521 (2001).
- ¹² Since x-ray spectrum data depend on not only the polar angle θ but also the azimuthal angle ϕ (which is in the a-b plane), in order to compare the data in the polycrystalline sample, one should average the data over both θ and ϕ . This explains why the spectrum at 45 degrees is different from the data in the polycrystalline sample. The averaged absorption spectrum represents the boron partial density of states. This is also the reason why all three set data in the polycrystalline or powder samples from different groups [Y. Zhu *et al.* Phys. Rev. Lett. **88**, 247002 (2002), T. A. Callcott *et al.* Phys. Rev. B **64**, 132504 (2001), and McGuinness *et al.*, Europhys. Lett. **56**, 112 (2001)] are consistent. In the sintered sample [McGuinness *et al.*, Europhys. Lett. **56**, 112 (2001)], as noted by those authors, surface boron oxides are more substantial and may significantly change the spectrum. Consequently their sinister MgB2 emission spectrum looks more similar to the B₂O₃ spectrum shown in Fig. 4 of the first paper of Ref. 5.
- ¹³ T. A. Callcott, E. T. Arakawa, and D. L. Ederer, Phys. Rev. B **18**, 6622 (1978); T. A. Callcott and D. L. Ederer, Phys. Rev. Lett. **62**, 1322 (1989).
- ¹⁴ J. Kortus *et al.*, Phys. Rev. Lett. **86**, 4366 (2001).
- ¹⁵ The self-absorption in our RIXS data is very weak. The reason is as follows. First, the self-absorption effect becomes stronger with increase in the incident angle as seen from the absorption spectra. Consequently, if the self-absorption had a strong contribution to our RIXS data, we would expect a monotonic decrease in the intensity of peak C. This does not agree with our experimental observation: the intensity of peak C decreases and after 45 degrees, it increases. Therefore, we conclude that the self-absorption effect less likely plays a dominant role in our RIXS spectra.
- ¹⁶ Y. Kong, O. V. Dolgov, O. Jepsen and O. K. Anderson, Phys. Rev. B **64**, 020501 (2001)

TABLE I. A comparison between experimental and theoretical energy positions for six peaks and valleys. The last column shows their corresponding crystal momenta and assigned special symmetry points. All the energies are referenced to the Fermi level.

Peak & valley	Experiment (eV)	Theory (eV)	Deviation (eV)	k -point
a	0.27	0.27	0.00	Γ_1
b	1.25	1.49	0.24	Γ_2
c	2.24	2.43	0.19	(0.38, 0.25, 0) (0.3, 0.3, 0)
d	2.83	2.96	0.13	(0.46, 0.09, 0)(M ₂) (0.28, 0.28, 0)
e	3.66	3.79	0.13	M ₃
f	6.65	6.55	-0.10	Γ , (A ₂)

TABLE II. The resonant inelastic peak positions for two different angles $\theta = 15^\circ$ and $\theta = 60^\circ$. At $\theta = 15^\circ$ the strong electron-phonon coupling in the flat σ band leads to a surprising enhancement of peak C at 187.30 eV. The energy units are in eV. The experimental uncertainty is about 0.2 eV.

Excitation energy	$\theta = 15^\circ$		$\theta = 60^\circ$	
A	B	C	B	C
187.50	185.05		185.05	
187.75	185.05	187.30	185.05	187.07
188.00	185.05	187.21	185.05	186.95
188.25	185.05	186.98	185.05	186.95

FIG. 1. Experimental geometry. A linearly polarized photon with energy ω_{in} is incident on the sample, and the outgoing photon energy becomes ω_{out} . \mathbf{n} is surface normal, \mathbf{E} is polarization of incident photon, $(a - b)$ is plane of boron atoms, and \mathbf{c} is normal to boron plane.

FIG. 2. (a) The angular-resolved experimental absorption spectra at the boron K -edge. θ represents the angle between the electric polarization \vec{E} and the $a - b$ plane. We scan from 15° to 45° with incremental angle of 7.5° . Six peaks and valleys are labeled by $a - f$. The experimental geometry is shown in the inset. (b) Theoretical spectra with the exact same condition. Two dashed curves represent results at 0 and 90° , respectively. (c) Band structure. Vertical short-dashed lines highlight the connection between the band structure and absorption spectra. Crossing points are denoted with a_1, a_2, a_3 , etc. The long vertical line represents the Fermi level which is set to zero.

FIG. 3. Transition-matrix element contour in the reciprocal space. The x axis denotes the k_x while the y axis the k_y axis. Four columns represent results for peaks a, c, d and f , respectively. The first and third rows are calculated at $\theta = 15^\circ$, while the second and fourth rows are at $\theta = 45^\circ$. The first and second rows are for the crystal momentum $k_z = 0$ while the third and fourth rows are for $k_z = 2\pi/c$. Numbers (in arbitrary units) near contours show the magnitude of transition matrix elements. The high symmetry points are shown in (a) and (c), and are also shown in 3-dimensional BZ.

FIG. 4. Unoccupied spatial charge density plot in the $y - z$ plane (the z axis is same as the c axis). (a) represents charge distribution for bands at point c_3 (see Fig. 1(c)) and other points c_2, d_2 and d_3 . The charge is mainly located around boron sites. (b) represents those bands at point c_4 (see Fig. 1(c)) as well as other points c_1, c_5, d_1, d_4 , and d_5 . The density is located around magnesium sites, which makes little contributions to our absorption spectra.

FIG. 5. Resonant inelastic x-ray scattering spectra measured at (a) $\theta = 15^\circ$ and (b) $\theta = 60^\circ$. The main difference is that at $\theta = 15^\circ$, there is an enhancement of the inelastic peak C at excitation energy of 187.75 eV. The Fermi energy is at about 187.28 eV.

FIG. 6. (a) Momentum transfer $\Delta\mathbf{k}$ in RIXS process. The projection of the momentum transfer along the a/b plane changes with the incident angle, with the minimum at 45° in our experimental geometry. \mathbf{k}_{in} and \mathbf{k}_{out} are incident and outgoing momenta, respectively. \mathbf{n} denotes the surface normal or the c axis. (b) With momentum transfer Δk , valence electrons from different bands can recombine with the core hole, showing a strong enhancement in the RIXS spectra (see Fig. 5(a)).

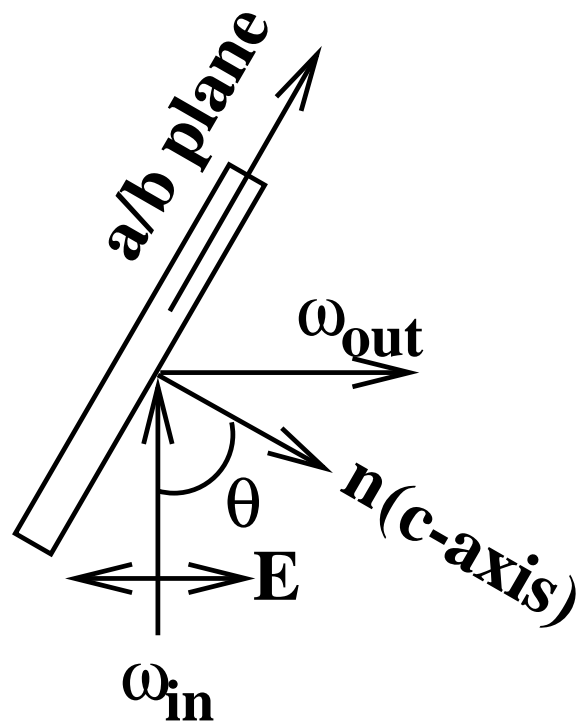


FIGURE 1

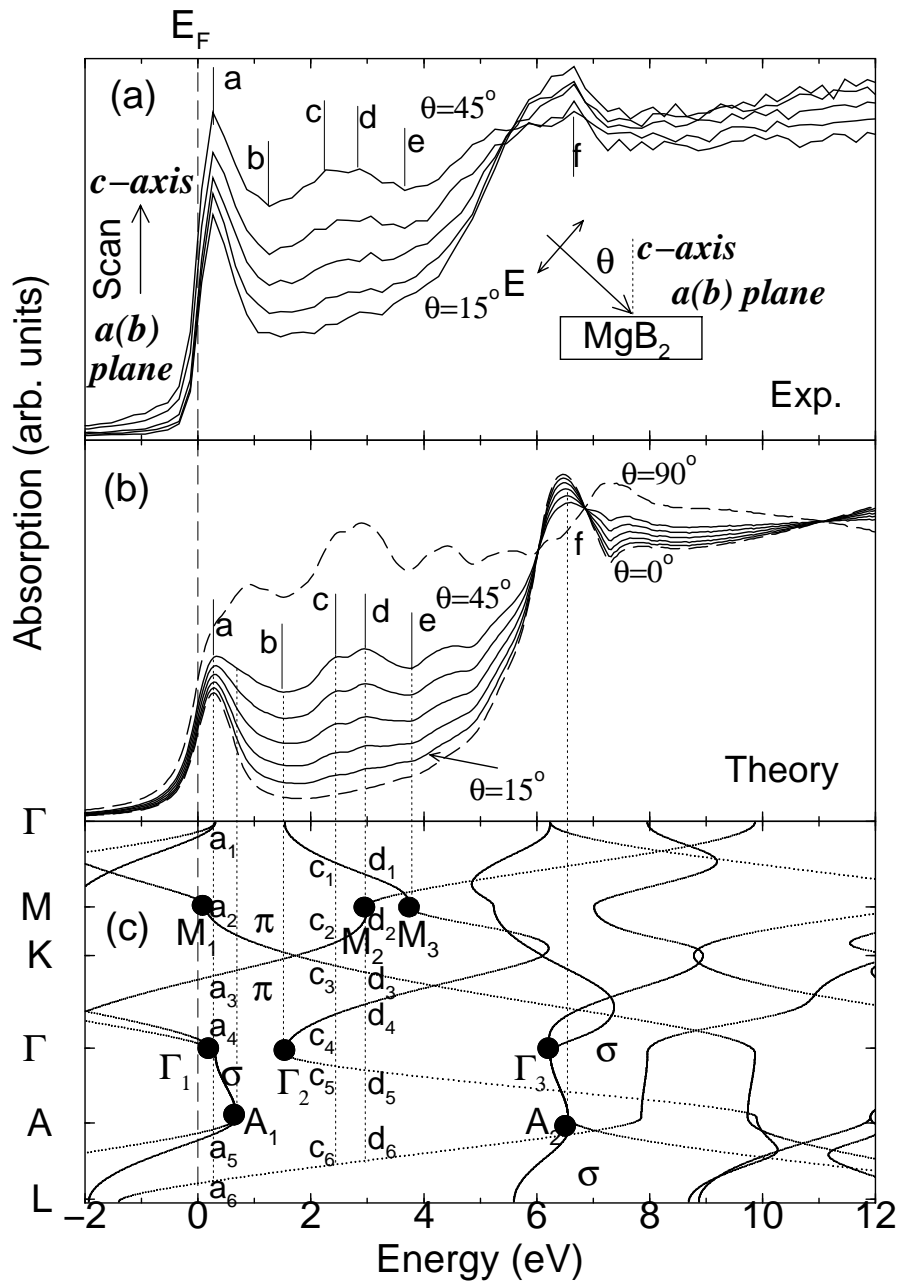


FIGURE 2

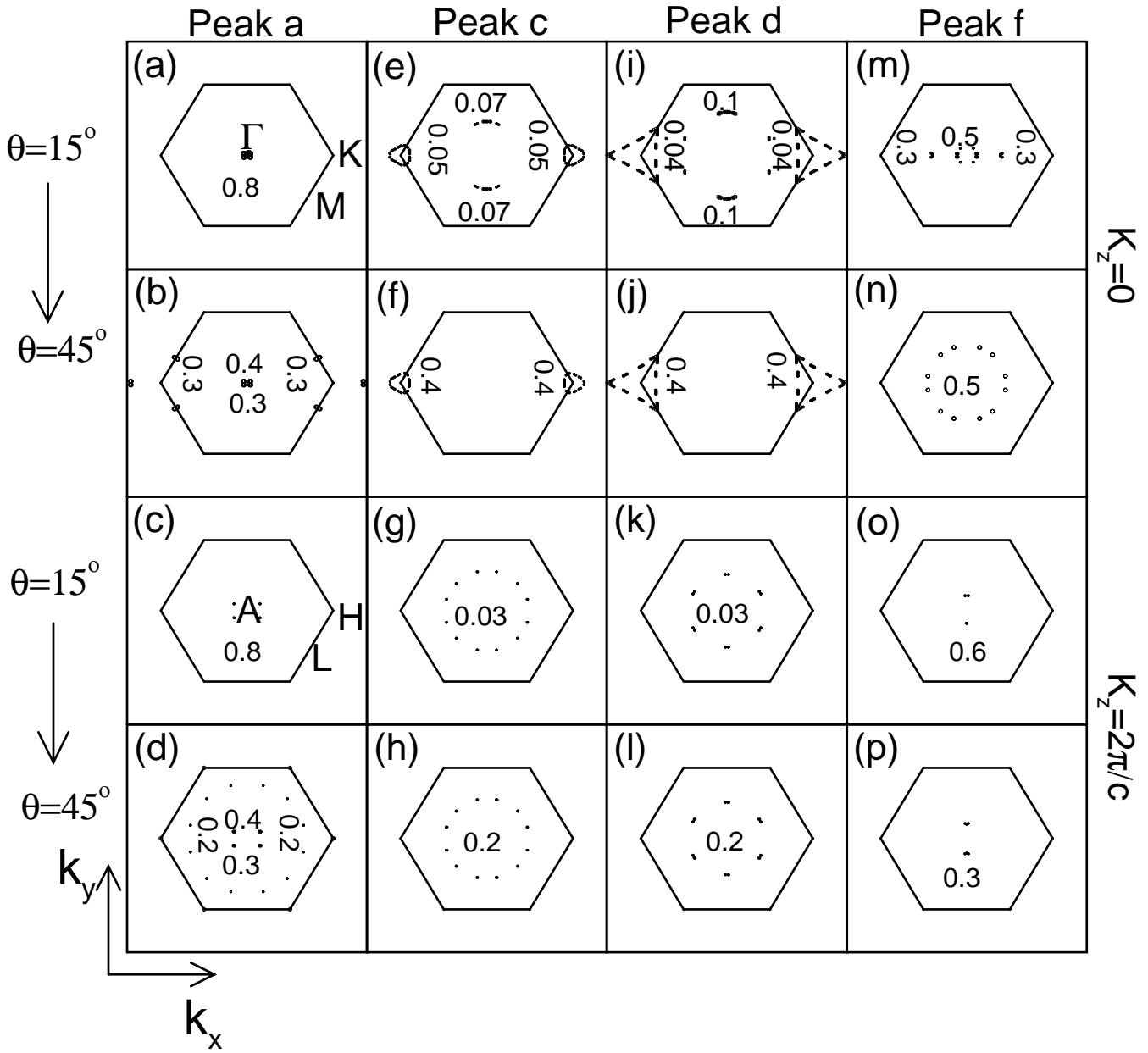
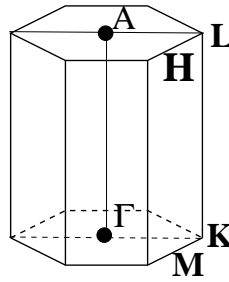


FIGURE 3

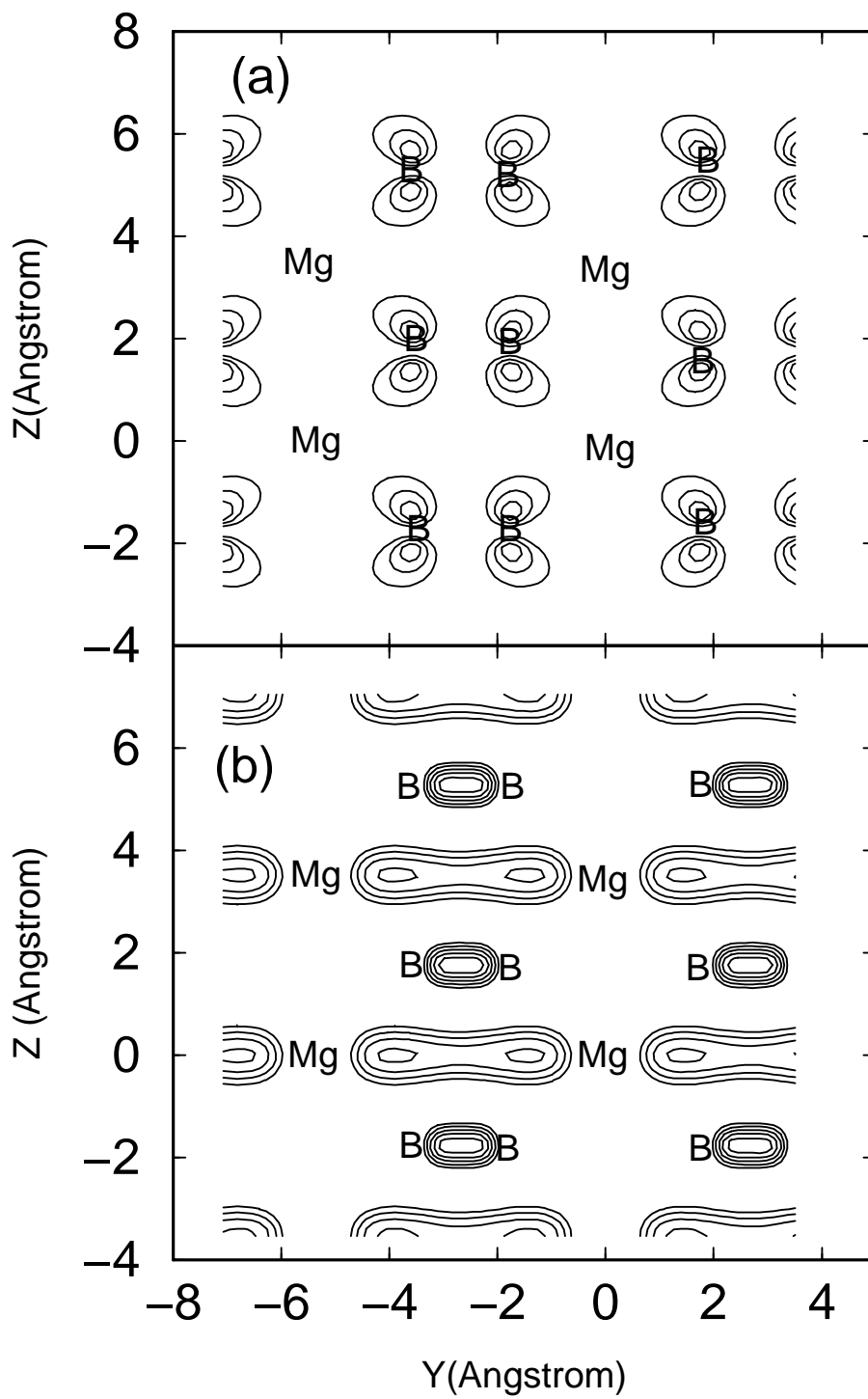


FIGURE 4

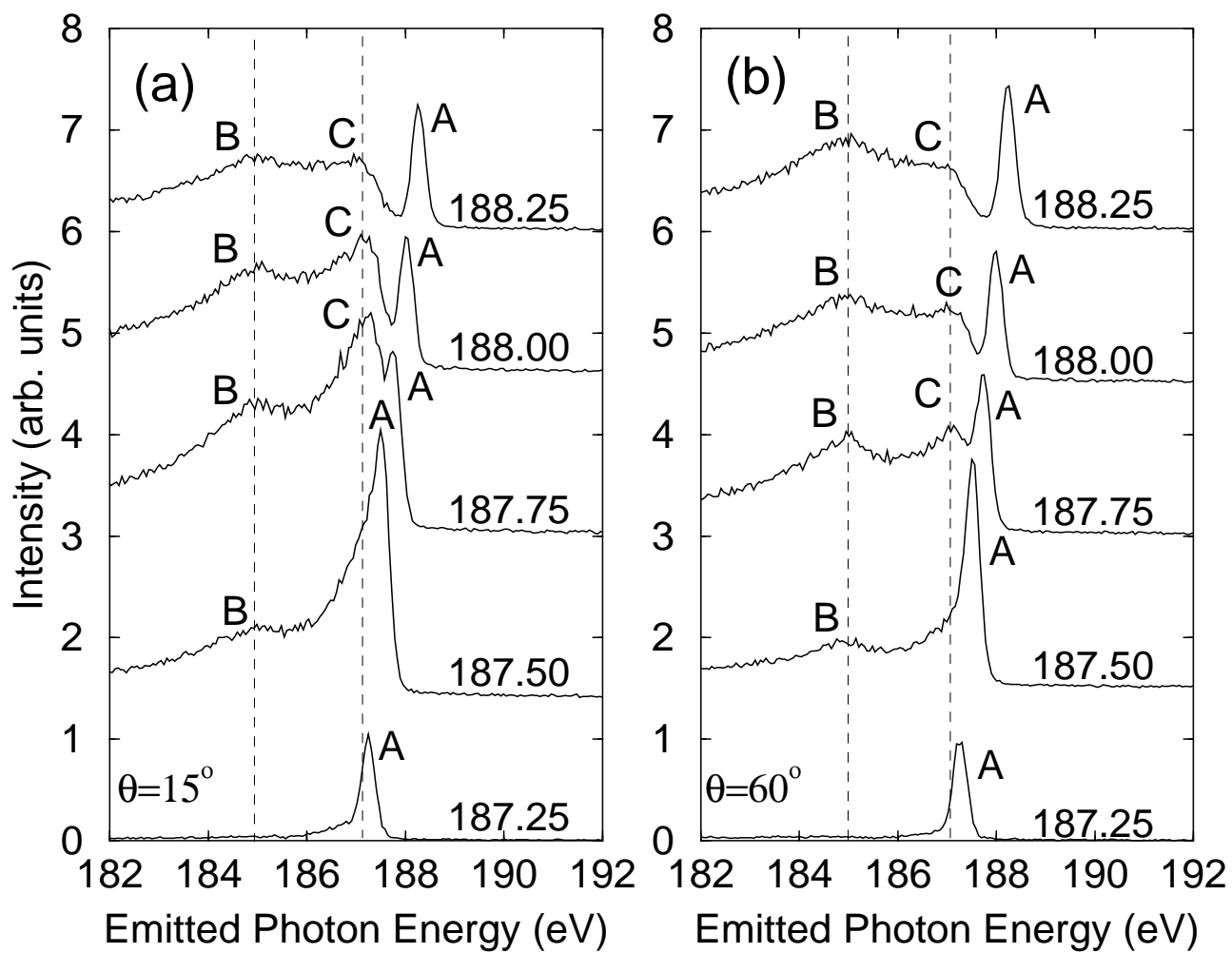
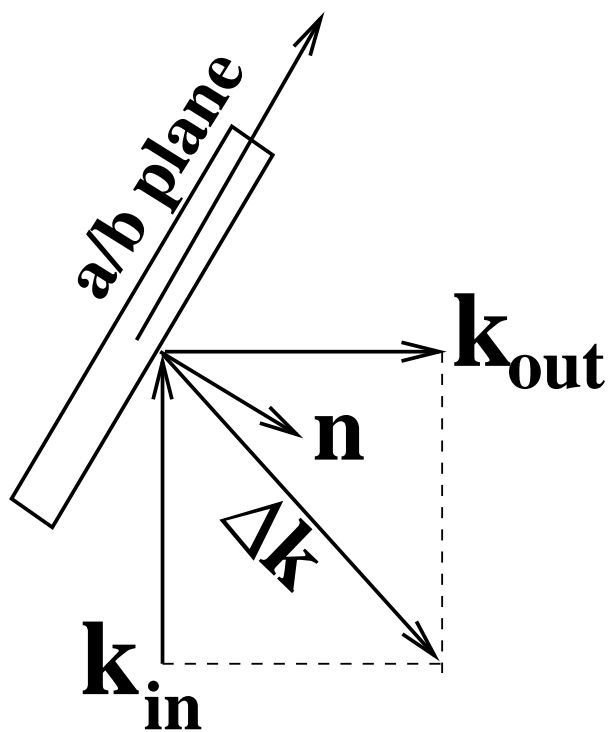


FIGURE 5

(a)



(b)

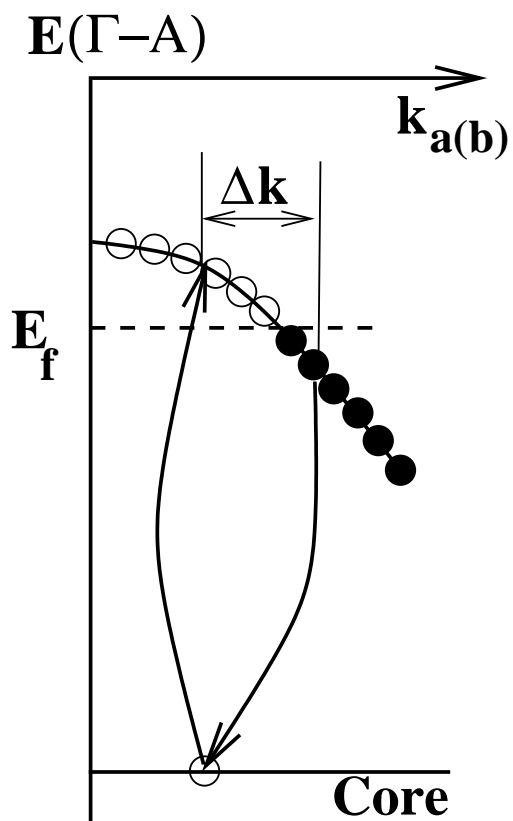


FIGURE 6